Degradation Behaviour of Lithium-Ion Batteries based on Field Measured Frequency Regulation Mission Profile

Stroe, Daniel Ioan; Swierczynski, Maciej Jozef; Stroe, Ana-Irina; Teodorescu, Remus; Lærke, Rasmus; Kjær, Philip Carne

Published in:
Proceedings of the 2015 IEEE Energy Conversion Congress and Exposition (ECCE)

DOI (link to publication from Publisher):
10.1109/ECCE.2015.7309663

Publication date:
2015

Document Version
Accepted author manuscript, peer reviewed version

Degradation Behaviour of Lithium-Ion Batteries based on Field Measured Frequency Regulation Mission Profile

Daniel-Ioan Stroe, Maciej Swierczynski, Ana-Irina Stroe, Remus Teodorescu
Department of Energy Technology, Aalborg University
Aalborg, Denmark
dis@et.aau.dk

Rasmus Laerke, Philip Carne Kjaer
Vestas Technology R&D
Aarhus, Denmark
pck@vestas.dk

***Abstract*—Energy storage systems based on Lithium-ion batteries have been proposed as an environmental friendly alternative to traditional conventional generating units for providing grid frequency regulation. One major challenge regarding the use of Lithium-ion batteries in such applications is their cost competitiveness in comparison to other storage technologies or with the traditional frequency regulation methods. In order to surpass this challenge and to allow for optimal sizing and proper use of the battery, accurate knowledge about the lifetime of the Lithium-ion battery and its degradation behaviour is required.**

This paper aims to investigate, based on a laboratory developed lifetime model, the degradation behaviour of the performance parameters (i.e., capacity and power capability) of a Lithium-ion battery cell when it is subjected to a field measured mission profile, which is characteristic to the primary frequency regulation service.

Keywords—Lithium-Ion Battery, Degradation, Frequency Regulation, Mission Profile

I. INTRODUCTION

Lithium-ion (Li-ion) batteries have become the standard choice for the e-mobility (e.g. plug-in hybrid electric vehicles, full electric vehicles etc.) and consumers applications (laptops, tablets etc.) because of their outstanding characteristics, which include high gravimetric and volumetric energy density, high operating voltage level, long calendar and cycle lifetime [1]. However, Li-ion batteries spread to other sectors such as grid support services and back-up power applications is still constrained by their cost competitiveness [2]. A solution to minimize this issue is to use the Li-ion batteries in a proper and efficient way i.e., avoiding operation regimes, which can cause fast degradation and inefficient use of the Li-ion battery. This can be realized by having accurate information about the battery's lifetime and its performance-degradation behaviour, which is caused by ageing.

Usually, information about the performance-degradation of the Li-ion batteries are obtained through accurate lifetime models. The Li-ion battery lifetime models are required from the planning stage of the project in order to allow for investment profitability calculations; an accurate lifetime model for the Li-ion battery will reduce the uncertainty of the business case. Furthermore, lifetime models are required because the main performance parameters (i.e., capacity and power capability) of Li-ion batteries are degrading with ageing [3], [4]. Thus, information about the ageing behaviour of these parameters becomes mandatory in order to ensure that the Li-ion battery energy storage system (ESS) will successfully deliver the service throughout its life and in order to avoid operation regimes, which are degrading the performance of the battery fast.

From technical perspective, due to their characteristics, Li-ion batteries can be used for a wide variety of stationary energy storage applications [1], [5]. However, one of the few applications, which at present might ensure economic viability of the investment in Li-ion batteries, for some markets, as is the case of Denmark, is the primary frequency regulation (PFR) [6].

The use of Li-ion batteries for providing PFR has been already studied from different perspectives. The sizing of a Li-ion battery ESS for providing PFR was discussed in [7]. Furthermore, different control strategies for providing PFR with Li-ion battery ESS were investigated in [8], [9]. Finally, lifetime studies of Li-ion batteries used in frequency regulation applications were carried out [8], [10]. However, in the former, the studies were performed either considering a synthetic generated frequency regulation mission profile (not a field measured one) or without considering a detailed Li-ion battery lifetime model. Both of these issues are surpassed in the present research

This paper aims to offer the reader a perspective on the degradation behaviour of certain Li-ion battery chemistry (i.e., $LiFePO_4/C$), when such batteries are used as part of an ESS, which is providing PFR on the Danish energy market. In order to perform this analysis, a lifetime model that is able to estimate the degradation behaviour of the performance parameters of a lithium ion phosphate ($LiFePO_4/C$) battery was developed based on accelerated ageing tests performed in laboratory. Furthermore, a one year mission profile (battery state-of-charge and temperature), which was measured on field

while the ESS based on $LiFePO_4/C$ had provided the PFR service, was utilized as a base for this analysis.

II. Frequency Regulation with Energy Storage Systems

A. Primary Frequency Regulation Charactseristics

The purpose of the frequency regulation service is to maintain the grid frequency within a predefined interval (e.g., 50Hz ± 0.02Hz) following a disturbance that was caused, or resulted in, a significant imbalance between generation and loads. To maintain the balance between generation and load, most of the transmission system operators (TSOs) are using three levels of controls and reserves, which are performed in successive steps [11]; this is also the case of the Danish TSO, Energinet.dk [12], which is considered in this paper. Nevertheless, this work focuses on the first level, namely, the PFR.

Traditionally, the PFR is provided by fast reacting conventional generating units (CGUs), which are online, by increasing or decreasing their production depending if under-frequencies or over-frequencies are detected, respectively. Nevertheless, in a world chasing for more environmentally friendly solutions, the use of energy storage systems based on Li-ion batteries for providing PFR has emerged as an alternative. Thus, the ESS will provide down-regulation (when over-frequencies, $f > 50.02$, are detected) by charging from the grid and up-regulation (when under-frequencies, $f < 49.98$, are detected) by discharging to the grid, as illustrated in Fig.1.

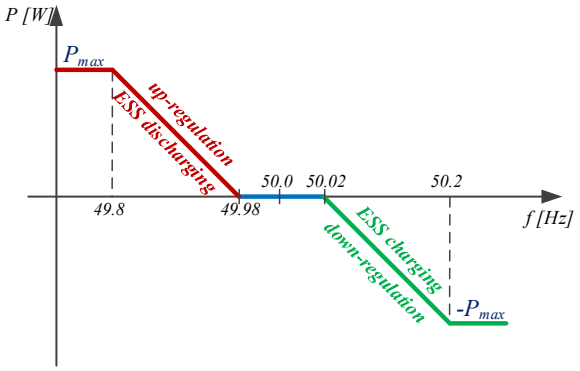

Fig. 1. Characteristic of PFR service in Denmark and action of the ESS according to the event.

According to the regulations imposed by the Energinet.dk, PFR is supplied if the grid frequency deviates up to ± 200 mHz from the reference frequency of 50 Hz. Nevertheless, a dead band of ± 20 mHz around the reference frequency is allowed, as shown in Fig. 1. The PFR service is delivered linearly, according to the droop presented in Fig. 1, at frequency deviations between ± 20 mHz and ± 200 mHz from the 50 Hz reference frequency. Furthermore, the first half of the reserve has to be supplied within 15 seconds after the deviation is recorded and the reserve has to be fully activated within 30 seconds for a frequency deviation of ± 200 mHz. Finally, the maximum power has to be supplied for a maximum of 15 minutes after which a break of 15 minutes is allowed for the reserve to be re-established [12]. It has to be highlighted that the aforementioned technical requirements are valid for all players participating into the PFR market and are not customized for ESSs; actually, at present there are no grid codes etc. for grid-connected ESS. For more detailed technical requirements regarding the PFR service, the reader is referred to [12].

B. PFR with Lithium-ion Batteries in Denmark

Due to their characteristics such as fast response, long lifetime at partial charge/discharge, high power capability during both charging and discharging, which are matching well the requirements of the PFR service, Li-ion batteries are evaluated in several pilot projects where ESS are used for providing the aforementioned service. This is also the case of the 1.6 MW/ 0.4 MWh ESS installed in Western Denmark, in conjunction with a 12 MW wind power plant (see Fig. 2), which actively participates in the PFR Market since 2013 [13], [14].

As illustrated in Fig. 2, the ESS is composed from two sub-systems (i.e., ESS1 – 0.4MW/ 0.1MWh and ESS2 – 1.2MW/ 0.3MWh), which are based on Li-ion batteries provided by two different suppliers. For this work, only ESS1 based on $LiFePO_4/C$ battery cells is of interest.

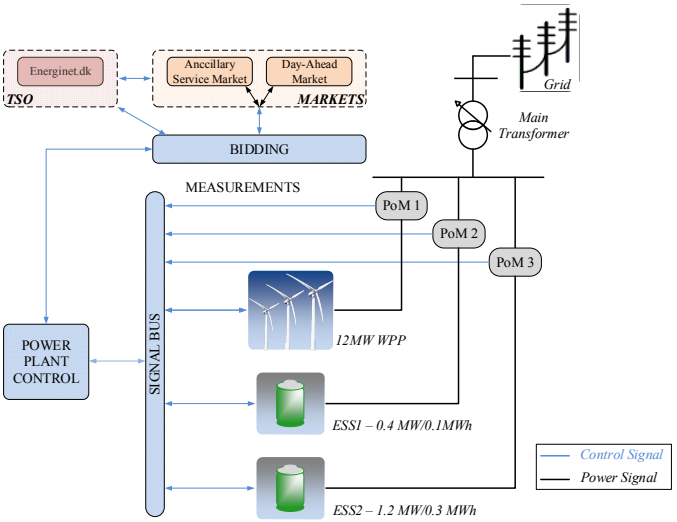

Fig. 2. Energy storage system and wind power connected to the grid [13].

Asymmetrical bids are allowed in the Danish energy market (i.e., up-regulation and down-regulation are treated separately) and higher revenues are generated by the upwards regulation [12]. Consequently, it was decided the ESS to participate only on the up-regulation market. Moreover, in order to bid maximum power and thus to maximize the revenues, the SOC of both systems is kept at 90% [13]. The SOC re-establishing (i.e., re-charging of the system to 90% SOC), after PFR service was delivered, is realized during periods of over-frequencies following the procedure presented in [13]. Furthermore, in the rare case when the under-frequencies persist for more than 15 minutes, the delivery of the PFR service is interrupted and a 15 minutes period for SOC re-establishing is granted to the ESS.

III. Energy Storage System Lifetime Model

A. $LiFePO_4$/C-based Batteries

The Li-ion battery family is vast and many Li-ion battery chemistries are available at present on the market; each of this chemistries has its own advantages and drawbacks, which makes it suitable or not for providing the PFR service [15]. As presented by Swierczynski et al. in [16], $LiFePO_4$/C battery chemistry is highly suitable for the discussed grid support service because of its characteristics such as long calendar and cycle lifetime, high power capability during both charging and discharging, and increased safety.

In order to perform the battery degradation behaviour analysis, a lifetime model was developed for similar $LiFePO_4$/C battery cells as the ones which are composing the grid-connected ESS1 (see Fig. 2). The basic electrical characteristics of these battery cells are summarized in Table I.

TABLE I. Electrical Parameters of the Tested $LiFePO_4$/C Battery Cell

Parameter	Value
Capacity [Ah]	2.5
Nominal voltage [V]	3.3
Maximum voltage [V]	3.6
Minimum voltage [V]	2.0
Max. continuous charge current [A]	10
Max. continuous discharge current [A]	70
Operating Temperature [°C]	-30 to 55
Storage Temperature [°C]	-40 to 60

B. Lithium-Ion Battery Lifetime Testing

The lifetime model of the $LiFePO_4$/C battery cell was developed based on results obtained from accelerated ageing tests. Because the performance of the Li-ion batteries are degrading during both periods of operation and storage (idling), accelerated calendar and cycle lifetime tests were performed in laboratory following the testing procedure presented in [3], in order to determine the ageing behaviour of the $LiFePO_4$/C battery cells at idling and cycle conditions, respectively. The accelerated calendar and cycling lifetime tests were carried out at the conditions presented in Fig. 3 and Fig. 4, respectively.

The two stress factors which are influencing the calendar lifetime of the Li-ion batteries are the storage SOC-level and the storage temperature, while the stress factors which are influencing the cycle lifetime of Li-ion batteries are the temperature, the cycle depth, the average SOC-level during the cycle and the charging/discharging current rate (C-rate). Nevertheless, all the accelerated cycle lifetime tests were performed considering a C-rate equal to 4C, which can be treated as a worst case scenario for the tested battery cells (4C-rate is the maximum continuous charging current that the battery can withstand). Furthermore, usually the stress factors have a non-linear effect on the lifetime of the Li-ion battery cells. Consequently, in order to accurately interpolate between the considered stress levels and to extrapolate the measured degradation of the performance parameters to the normal operating stress levels, three stress levels where considered for each stress factor as it can be seen in Fig. 3 and Fig. 4. Finally, any possible interaction between stress factors and their corresponding stress levels were disregarded.

Most of the accelerated ageing tests summarized in Fig. 3 and Fig. 4 were performed until the tested $LiFePO_4$/C battery cell reached the end-of-life (EOL) criterion of 20% capacity fade [17]. Nevertheless, since the ageing of the studied battery cells was found to be a slow process for certain conditions, the measured capacity fade characteristics for that cases (when EOL criterion had not been reached) was extrapolated until the predefined EOL criterion was reached.

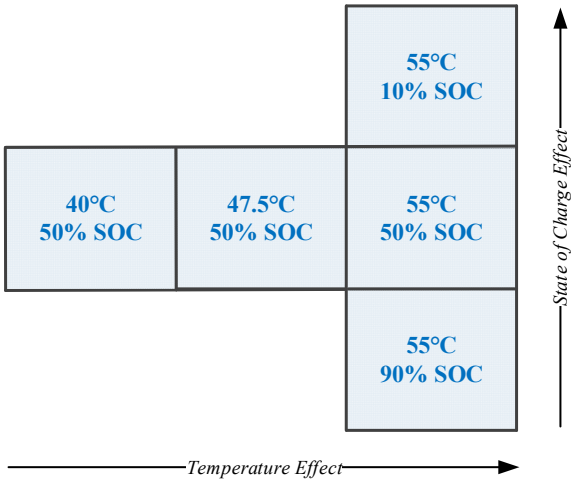

Fig. 3. Test matrix for determining the calendar lifetime of the tested $LiFePO_4$/C battery cells.

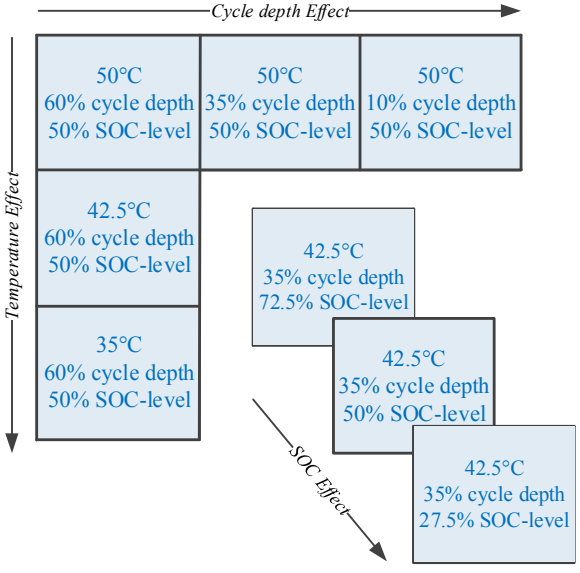

Fig. 4. Test matrix for determining the cycle lifetime of the tested $LiFePO_4$/C battery cells.

C. Lithium-Ion Battery Lifetime Model

Lifetime models, which are able to predict the degradation behaviour of the performance parameters (i.e., capacity and power capability) of the $LiFePO_4$/C cells, were developed and parametrized based on the results obtained from the accelerated lifetime tests. Separate lifetime models were developed for the calendar ageing and for cycle ageing dimensions. The battery cells' power capability was computed as described in [3].

Based on the obtained accelerated calendar ageing results, calendar lifetime models, which are able to estimate the capacity fade and the power capability decrease of the $LiFePO_4$/C battery cells for idling at different temperatures and for all SOCs, were developed. However, the Li-ion batteries used in grid support services are most of the time operated at 25°C (for optimum performance and increased lifetime) by means of air-conditioning systems. Therefore, in order to illustrate this constraint, the models given in (1) and (2) present the degradation of the two performance parameters for a storage temperature of 25°C.

$$C_{f\_cal} = 0.1723 \cdot e^{0.007388 \cdot SOC} \cdot t^{0.8} \quad (1)$$

$$PC_{d\_cal} = 0.0033 \cdot SOC^{0.4513} \cdot t \quad (2)$$

Where, *SOC* represents the storage SOC-level, *t* represents the storage time, expressed in months, and C_{f_cal} and PC_{d_cal} represent the capacity fade and power capability decrease during storage, respectively.

Considering the developed calendar lifetime models, the capacity fade and power capability decrease can be estimated for any storage SOC-level. An example is given in Fig. 5 and Fig. 6, where the degradation behaviour of the capacity and of the power capability is presented, respectively, for storage at 25°C and three different SOC-levels (i.e., 10%, 50%, and 90%). Furthermore, the estimated monthly degradation (i.e., correction factor) of the two parameters for the considered storage conditions are also illustrated in Fig. 5 and Fig. 6; respectively; by continuously summing up the values of the correction factors, the battery degradation is calculated at each model iteration step.

As it can be observed in Fig. 5, the capacity fade of the tested $LiFePO_4$/C battery cells depends non-linearly on the storage time, with a tendency of slowing-down, while the ageing process evolves; on the contrary, the power capability decrease of the $LiFePO_4$/C battery cells follows a linear dependence on the storage time. Moreover, by comparing the results presented in Fig. 5 and Fig. 6 it can be concluded that the capacity of the tested battery cells degrades much faster than the power capability, independent on the considered idling conditions.

Based on the results obtained from the performed accelerated cycle ageing tests, lifetime models that are able to estimate the capacity fade and the power capability decrease of the $LiFePO_4$/C battery cell for cycling at various conditions, were developed and given by (3) and (4) for a cycling temperature of 25°C.

$$C_{f\_cyc} = 0.021 \cdot e^{-0.01943 \cdot SOC} \cdot cd^{0.7162} \cdot nc^{0.5} \quad (3)$$

$$PC_{d\_cyc} = 1.1725 \cdot 10^{-6} \cdot cd^{0.7891} \cdot nc \quad (4)$$

Where, *SOC* represents the average SOC level during the cycle, *cd* represents the depth of the cycle, *nc* represents the number of cycles, and C_{f_cyc} and PC_{d_cyc} represent the capacity fade and power capability decrease during cycling, respectively

Fig.7 and Fig. 8 are presenting the estimated degradation behaviour of the capacity and of the power capability when the Li-ion battery cells are cycled at 25 °C with three different cycle depths (i.e., 30%, 70% and 100% (full cycle)). It was found out that the capacity fade of the tested $LiFePO_4$/C battery cells follows a square-root function on the number of performed cycles, while the power capability depends linearly on the number of cycles. Furthermore, similarly to the case of calendar ageing, the capacity of the cells degrades faster than the power capability independent on the cycle conditions.

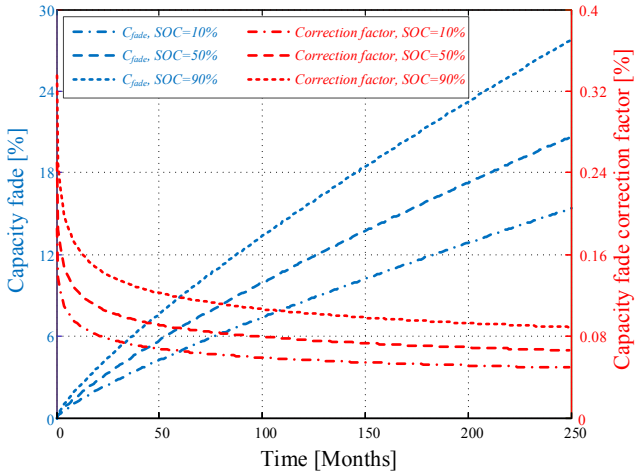

Fig. 5. Estimated capacity fade and corresponding capacity fade correction factors for storage at 25°C and different SOC-levels.

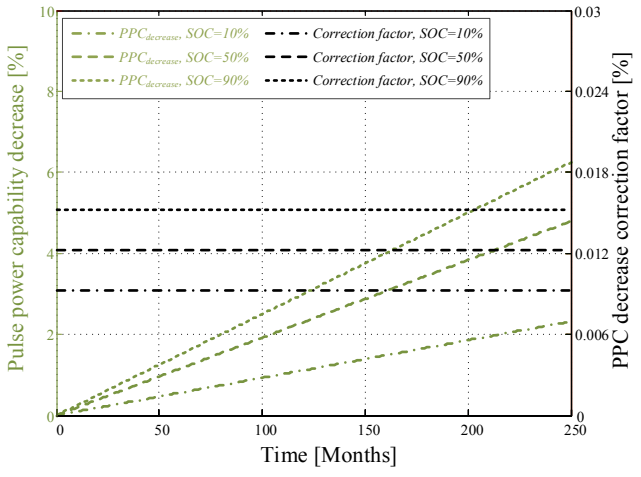

Fig. 6. Estimated power capability decrease and corresponding power capability decrease correction factors for storage at 25°C and different SOC-levels.

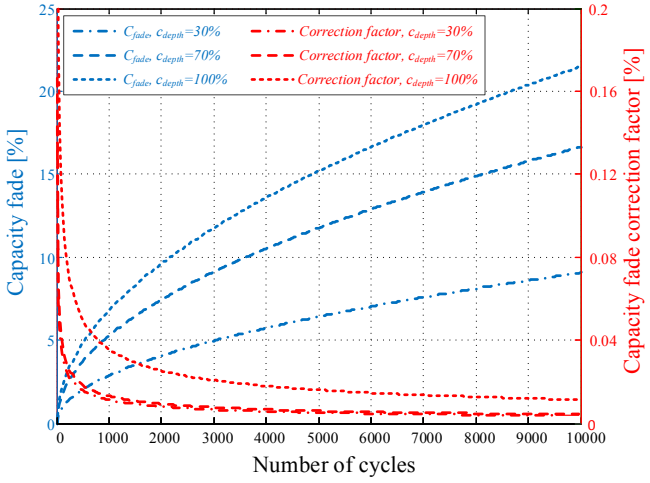

Fig. 7. Estimated capacity fade and corresponding capacity fade correction factors for cycling at 25°C with different cycle depths.

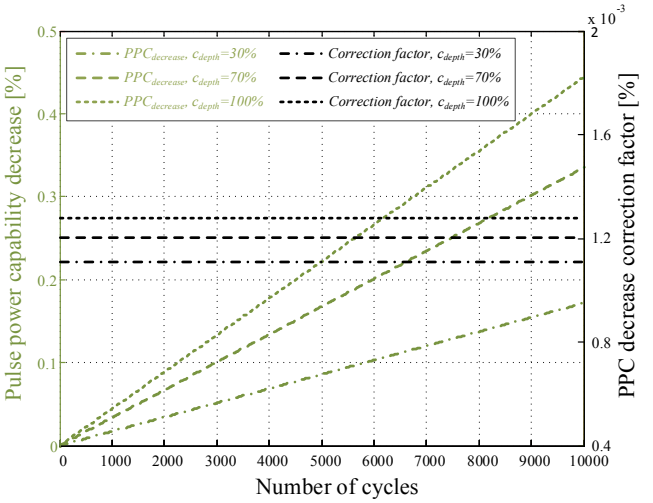

Fig. 8. Estimated power capability decrease and corresponding power capability decrease correction factors for cycling at 25°C with different cycle depths.

For a detailed analysis of the ageing behaviour of the considered Li-ion cells, the reader is referred to [17].

The proposed structure of the lifetime model for determining the ageing behaviour of the $LiFePO_4$/C battery cells independent on the mission profile is presented in Fig. 9. The input of the lifetime model is represented by the mission profile to which the battery is subjected to; the mission profile has two components, the SOC mission profile and the temperature mission profile. The proposed lifetime model returns at its output information about the degradation behaviour of the battery cells, by offering instantaneous information about the capacity fade and power capability decrease; based on these two parameters, the state-of-health (SOH) and the remaining useful lifetime (RUL) of the battery can be calculated, according to (5) and (6).

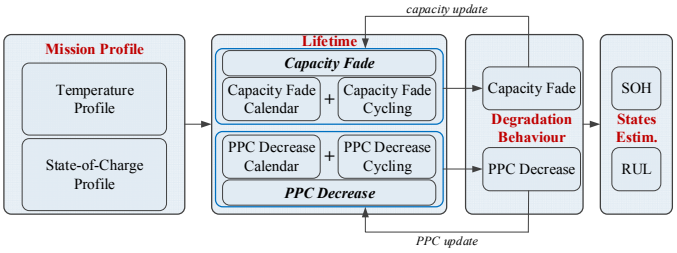

Fig. 9. Schematic representation of the proposed lifetime model.

$$SOH = \frac{C_{fade-actual}}{C_{fade-EOL}} \quad (5)$$

$$RUL = \frac{C_{fade-EOL}}{C_{fade-year}} \quad (6)$$

Where, $C_{fade\text{-}actual}$ represents the present capacity fade, $C_{fade\text{-}EOL}$ represents the capacity fade for the EOL criterion (e.g. 20%), and $C_{fade\text{-}year}$ represents the capacity fade during one year.

As it is presented in Fig. 5 – Fig. 8, the performance parameters of the battery cell are degrading in time following various nonlinear characteristics (for this specific battery cell, only valid for the capacity fade). This suggested that the same mission profile does not cause the same degradation to the performance parameters of the battery cell if it is applied at the cells' BOL or for an already aged cell. Consequently, in order to obtain reliable lifetime estimations, the performance parameters have to be updated after each iteration of the incremental lifetime calculations (see the feedback-arrows graphically illustrated in Fig. 9).

IV. Field Measured Mission Profile

For the degradation behaviour analysis, a one year field-measured mission profile corresponding to ESS1 (see Fig. 2) delivering the PFR service was considered. Based on own grid frequency measurements and considering the PFR control strategy discussed in [4], the SOC mission profile which was measured on the $LiFePO_4$/C-based ESS1 is presented in Fig. 10. Moreover, the temperature mission profile measured over a period of one month is illustrated in Fig. 11.

The $LiFePO_4$/C batteries composing the ESS1 are air cooled during both operation and stand-by. Consequently, their temperature varies in a narrow interval (22-26°C) as illustrated in Fig. 11, with a monthly average temperature of 23.18°C. Therefore, a constant temperature of 25°C was considered for the performed ageing behaviour analysis. Furthermore, in order to be applied to the developed lifetime models, the SOC mission profile was divided into the calendar and cycling components. Thus, it was found out that ESS1 was for almost 85% of the time on stand-by (idling), while the rest of the time it was providing PFR. Furthermore, using the rainflow cycle counting algorithm [18], the cycling mission profile was decomposed into cycles of different depths and average SOC-

levels. Fig. 12 illustrates the cycles distributed according to their cycle depths and average SOC-levels.

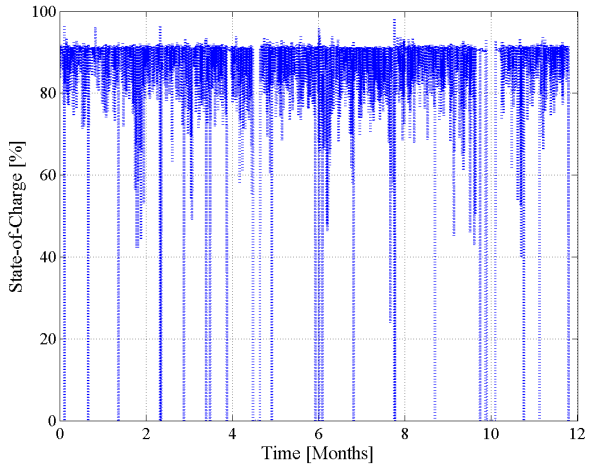

Fig. 10. One year SOC profile measured on $LiFePO_4$/C based ESS1 delivering PFR.

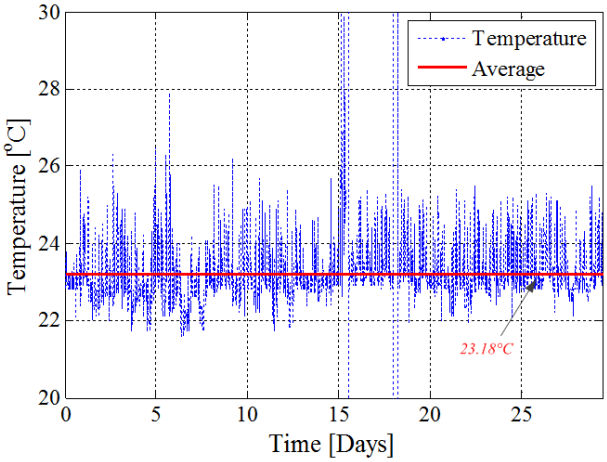

Fig. 11. One month temperature profile measured on $LiFePO_4$/C based ESS1 delivering PFR.

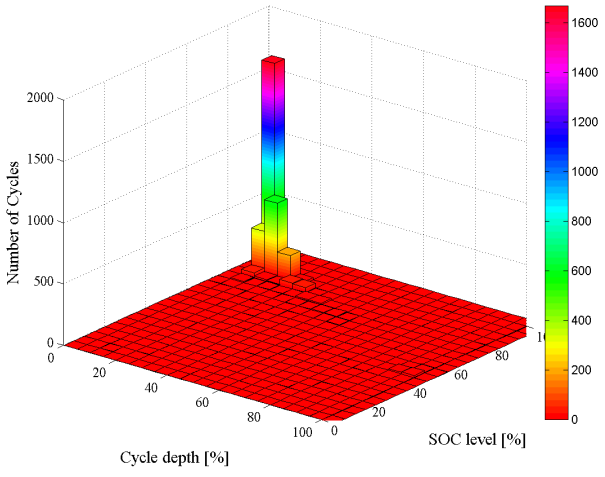

Fig. 12. Distribution of cycles according to their cycle depth and average SOC, corresponding to the SOC profile presented in Fig. 10.

V. Degradation Behaviour

In order to obtain the degradation behaviour (in terms of capacity and power capability) of the studied $LiFePO_4$/C battery cells, the SOC mission profile presented in Fig.10 was applied at the input of the developed lifetime model, while the temperature was considered constant at 25°C during the whole lifetime. Because the SOC mission profile was available only for a period of one year, this SOC profile was continuously applied to the lifetime model until the battery cells have reached the EOL criterion which was predefined at 20% capacity fade. Furthermore, the values of the capacity fade and of the power capability decrease were updated after each month of simulation. The estimated calendar and cycle capacity fade for each month during the first year of the simulation are presented in Fig. 13.

By summing up the monthly estimated capacity fade, the incremental capacity fade of the $LiFePO_4$/C battery cells was obtained and is presented in Fig. 13; for this estimation, a resolution of one month was considered. The total estimated incremental capacity fade caused by the PFR operation was computed by summing up the contribution of the monthly accumulated cycling and calendar capacity fade, respectively. The same procedure was applied to compute the incremental power capability decrease of the $LiFePO_4$/C battery cells (see Fig. 14) when they were subjected to the considered PFR mission profile

For the considered 20% capacity fade EOL criterion, it was found out that the considered $LiFePO_4$/C battery cells would survive approx. 10 years for the considered PFR profile. The main contribution to the overall capacity fade of the battery cells came from the calendar ageing component (idling operation). The calendar capacity fade rate was mainly accelerated by the idling operation at high SOC (i.e., 90% SOC as imposed by the considered control strategy [4]), because the capacity fade is accelerated by idling the tested cells at high SOC-levels, as shown in Fig. 5. The estimated power capability decrease, of the studied $LiFePO_4$/C battery cells, until the EOL has been reached, was approximately 3.25%; similar to the case of the capacity fade, the main contribution (i.e., 3%) to the power capability decrease came from the calendar ageing dimension.

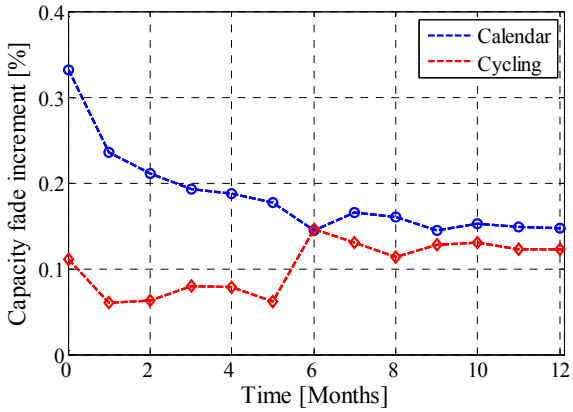

Fig. 13. Monthly capacity fade of the $LiFePO_4$/C battery cell caused by the field measured SOC profile illustrated in Fig. 10.

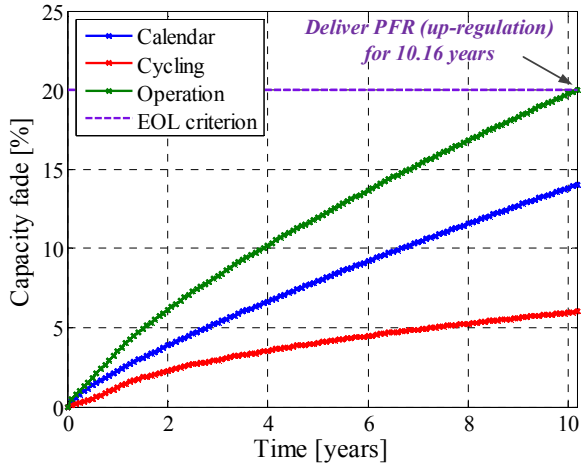

Fig. 14. Capacity fade of the $LiFePO_4$/C battery cells subjected to the PFR mission profile.

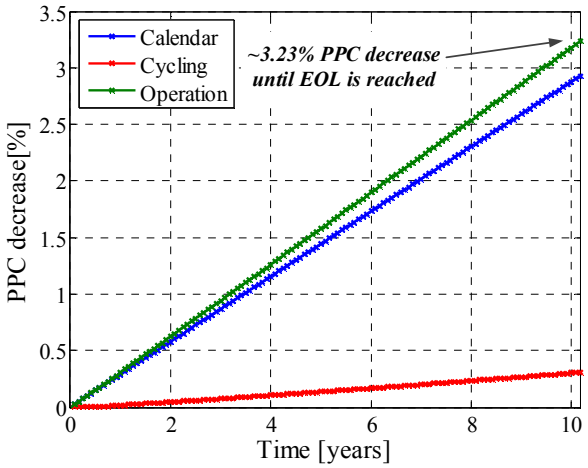

Fig. 15. Power capability decrease of the $LiFePO_4$/C battery cells subjected to the PFR mission profile

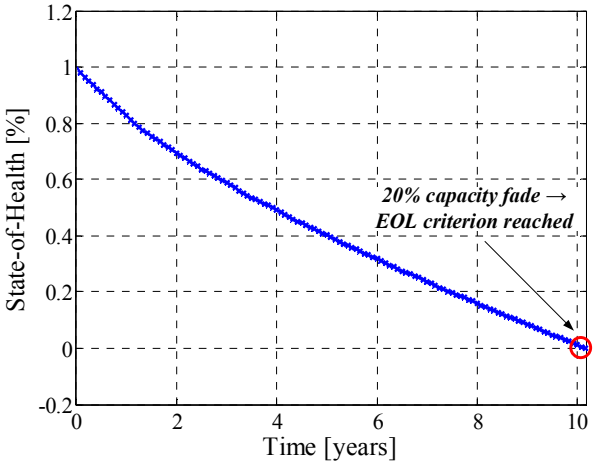

Fig. 16. SOH evolution of the $LiFePO_4$/C battery cells subjected to the PFR mission profile.

As presented in Fig. 9, from the estimated capacity fade and power capability decrease characteristics, the SOH of the battery cell can be predicted at every time instant. Nevertheless, as it was illustrated in Fig. 5 – Fig. 8, the capacity of tested $LiFePO_4$/C battery cells was degrading much faster than their power capability. Consequently, the SOH of the cells was related during whole simulation only with the batteries' capacity fade as given in (5) and is presented in Fig. 16.

VI. Conclusion

This paper has investigated the degradation behaviour of $LiFePO_4$/C battery cells when such batteries are used to provide PFR in the Danish energy market. For performing a reliable analysis a lifetime model was developed for the studied battery cells and a field measured mission profile characteristic to the PFR application was considered. By applying the PFR mission profile to the proposed $LiFePO_4$/C battery cell lifetime model it was observed that the capacity is the performance parameter, which limited the lifetime of the studied battery cells and not the power capability. The main contribution to the estimated capacity fade came from the calendar dimension; the calendar capacity fade was accelerated by the operating conditions that involve idling the $LiFePO_4$/C battery cell at a high SOC-level. Consequently, the lifetime of the studied battery cell might be enhanced by decreasing the idling SOC-level to values lower than 90%; however, this decrease of the idling SOC-level would decrease the revenues obtained from the up-regulation service since less power would be bid in the market. Nevertheless, for the considered field-measured PFR mission profile and with the existing PFR energy management strategy, the $LiFePO_4$/C would be able to fulfil the up-regulation service for a period of approx. 10 years before the EOL criterion would be reached.

Acknowledgment

This work was part of the "Intelligent Energy management System for a Virtual Power Plant" research project, which was founded by the Danish National Advanced Technology Foundation (HTF), Vestas Wind Systems A/S, and Aalborg University.

References

[1] B. Dunn, H. Kamath, and J.-M. Tarascon, "Electrical energy storage for the grid: A battery of choices," Science, vol. 334, pp. 928–935, 2011.

[2] Grid Energy Storage. US Department of Energy, December 2013.

[3] D.-I. Stroe, M. Swierczynski, A.-I. Stan, R. Teodorescu, S. J. Andreasen, "Accelerated lifetime testing methodology for lifetime estimation of Lithium-ion batteries used in augmented wind power plants," Industry Applications, IEEE Transactions on , vol.50, no.6, pp.4006,4017, Nov.-Dec. 2014.

[4] M. Ecker et al., "Calendar and cycle life study of $Li(NiMnCo)O_2$-based 18650 lithium-ion batteries," Journal of Power Sources, vol. 248, pp. 839-851, 2014.

[5] "Electric Energy Storage Technology Options: A Whithe Paper Primer on Applications, Costs, and Benefits," EPRI, Palo Alto, CA, 2010. 1020676.

[6] P. Braun, M. Swierczynski, R. Diosi, D.-I. Stroe, and R. Teodorescu, "Optimzing a Hybrid Energy Storage System for a Virtual Power Plant for Improved Wind Power Generation: A Case Study for Denmark," 6th International Renewable Energy Storage Conference and Exhibition, IRES 2011.

[7] P. Mercier, R. Cherkaoui, A. Oudalov, "Optimizing a Battery Energy Storage System for Frequency Control Application in an Isolated Power System," Power Systems, IEEE Transactions on, vol. 24, no.3, pp.1469-1477, Aug. 2009.

[8] E. Thorbergsson, V. Knap, M. Swierczynski, D.-I. Stroe, R. Teodorescu, "Primary Frequency Regulation with Li-Ion Battery Energy Storage System – Evaluation and Comparison of Different Control Strategies," 35th International Telecomunications Energy Conference, INTELEC 2013.

[9] B. Xu, A. Oudalov, J. Poland, A. Ulbig, G. Andersson, "BESS Control Strategies for Participating in Grid Frequency Regulation," 19th World Congress of the International Federation of Automatic Control, Cape Town, South Africa, August 2014.

[10] M. Swierczynski, D.-I. Stroe, A.-I. Stan, R. Teodorescu, "Primary frequency regulation with Li-ion battery energy storage system: A case study for Denmark," ECCE Asia Downunder (ECCE Asia), 2013 IEEE, pp. 487-492, 3-6 June 2013.

[11] Y.G. Rebours, D.S. Kirschen, M. Trotignon, and S. Rossignol, "A survey of frequency and voltage control ancillary services - Part I: Technical features," Power Systems, IEEE Transactions on, 22(1):350--357, Feb 2007.

[12] Energinet.dk. Ancillary services to be delivered in Denmark. Tender conditions. Technical Report Doc. 8871/11 v3, Case 10/2932, Fredericia, Denmark, 2012.

[13] M. Swierczynski et al., "Field Experience from Li-Ion BESS Delivering Primary Frequency Regulation in the Danish Energy Market," ECS Transactions, vol. 61, no. 37, pp. 1-14, 2014.

[14] P.C. Kjaer, R. Larke, and G.C. Tarnowski, "Ancillary services provided from wind power plant augmented with energy storage," Power Electronics and Applications (EPE), 2013 15th European Conference on, pages 1--7, Sept 2013.

[15] A.-I. Stan, M. Swierczynski, D.-I. Stroe, R. Teodorescu, S. J. Andreasen, "Lithium ion battery chemistries from renewable energy storage to automotive and back-up power applications — An overview," Optimization of Electrical and Electronic Equipment (OPTIM), 2014 International Conference on, pp. 713-720, 22-24 May 2014.

[16] M. Swierczynski, D.-I. Stroe, A.-I. Stan, R. Teodorescu, D.U. Sauer, "election and Performance-Degradation Modeling of $LiMO_2/Li_4Ti_5O_{12}$ and $LiFePO_4$/C Battery Cells as Suitable Energy Storage Systems for Grid Integration With Wind Power Plants: An Example for the Primary Frequency Regulation Service," Sustainable Energy, IEEE Transactions on , vol.5, no.1, pp.90-101, Jan. 2014

[17] D.-I. Stroe, "Lifetime models for Lithium-ion batteries used in virtual power plant applications," PhD Thesis, Aalborg University, 2014.

[18] C. Amzallag, J.P. Perry, J.L. Robert, J. Bahuad, "Standardisation of the rainflow counting method for fatigue analysis," International Journal of Fatigue, vol. 16, pp. 287-293, June 1994.